Cover Page

Universiteit Leiden

The handle http://hdl.handle.net/1887/78557 holds various files of this Leiden University dissertation.
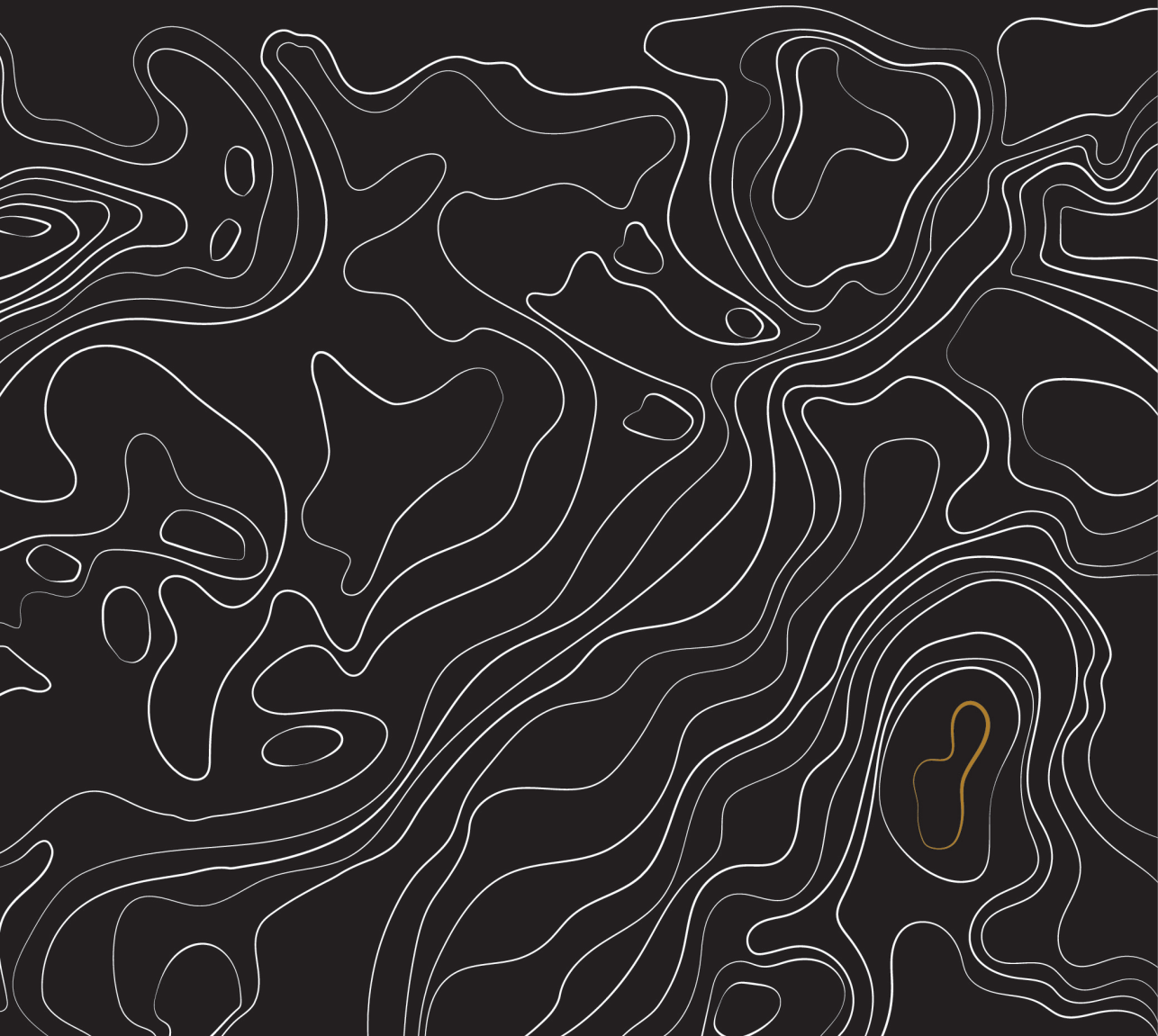
Author: Dinis Fernandes, C.
Title: Multi-parametric MRI to guide salvage treatment of recurrent prostate cancer
Issue Date: 2019-09-25

PART 2

Magnetic resonance imaging for the diagnosis and localisation of recurrent prostate cancer

4

QUANTITATIVE 3T MULTI-PARAMETRIC MRI OF BENIGN AND MALIGNANT PROSTATIC TISSUE IN PATIENTS WITH AND WITHOUT LOCAL RECURRENT PROSTATE CANCER AFTER EXTERNAL-BEAM RADIATION THERAPY

Catarina Dinis Fernandes[1]
Petra J van Houdt[1]
Stijn WTPJ Heijmink[2]
Iris Walraven[1]
Rick Keesman[1]
Milena Smolic[1]
Ghazaleh Ghobadi[1]
Henk G van der Poel[3]
Ivo G Schoots[2]
Floris J Pos[1]
Uulke A van der Heide[1]

[1]Department of Radiation Oncology, [2]Radiology and [3]Urology
The Netherlands Cancer Institute, Amsterdam, The Netherlands

ABSTRACT

Background: Post–radiotherapy locally recurrent prostate cancer (PCa) patients are candidates for focal salvage treatment. Multi–parametric MRI (mp-MRI) is attractive for tumour localisation. However, radiotherapy–induced tissue changes complicate image interpretation. To develop focal salvage strategies, accurate tumour localisation and distinction from benign tissue is necessary.

Purpose: To quantitatively characterise radio–recurrent tumour and benign radiation–induced changes using mp–MRI, and investigate which sequences optimise the distinction between tumour and benign surroundings.

Study type: Prospective case–control.

Subjects: Thirty-three patients with biochemical failure after external–beam radiotherapy (cases), 35 patients without post–radiotherapy recurrent disease (controls), and 13 patients with primary PCa (untreated).

Field Strength/ Sequences: 3T; quantitative mp–MRI: T_2-mapping, ADC, and K^{trans} and k_{ep} maps.

Assessment: Quantitative image-analysis of prostatic regions, within and between cases, controls, and untreated patients.

Statistical Tests: Within-groups: non–parametric Friedman analysis of variance with post-hoc Wilcoxon signed-rank tests; between-groups: Mann–Whitney tests. All with Bonferroni corrections. Generalised linear mixed modelling to ascertain the contribution of each map and location to tumour likelihood.

Results: Benign imaging values were comparable between cases and controls (P = 0.15 for ADC in the central gland up to 0.91 for k_{ep} in the peripheral zone), both with similarly high peri–urethral K^{trans} and k_{ep} values (min^{-1}) (median [range]: K^{trans} = 0.22 [0.14–0.43] and 0.22 [0.14–0.36], P = 0.60, k_{ep} = 0.43 [0.24–0.57] and 0.48 [0.32–0.67], P = 0.05). After radiotherapy, benign central gland values were significantly decreased for all maps (P ⩽ 0.001) as

well as T_2, K^{trans}, and k_{ep} of benign peripheral zone (all with $P \leqslant 0.002$). All imaging maps distinguished recurrent tumour from benign peripheral zone, but only ADC, K^{trans}, and k_{ep} were able to distinguish it from benign central gland. Recurrent tumour and peri-urethral K^{trans} values were not significantly different ($P = 0.81$), but k_{ep} values were ($P \leqslant 0.001$). Combining all quantitative maps and voxel location resulted in an optimal distinction between tumour and benign voxels.

Data Conclusion: Mp-MRI can distinguish recurrent tumour from benign tissue.

4.1 INTRODUCTION

One of the main treatment options for localised prostate cancer (PCa) is external-beam radiotherapy (EBRT). Depending on the risk-group, 5-year disease free survival varies from 67 to 80% for PCa patients who are treated with whole-gland radiotherapy (RT) to 78 Gy [58]. A small but significant proportion of patients failing the primary treatment, will harbour locally recurrent disease only [26, 27], for which focal treatment strategies, targeting the tumour region while sparing the surrounding uncompromised tissue, might offer a curative treatment option. To this end, multi-parametric magnetic resonance imaging (mp-MRI) with both anatomical and functional properties is attractive for loco-regional evaluation of recurrent PCa and for tumour boundary definition. However, RT-induced tissue changes pose a challenge to MRI interpretation. T2-weighted (T2w) MRI is the reference anatomical sequence, however it has limited performance in this setting as tumour conspicuity is decreased and zonal anatomy is often lost [37]. The use of functional sequences such as 1.5T MR spectroscopy [45] as well as diffusion weighted imaging (DWI) and dynamic contrast enhanced (DCE)-MRI [38–40] were found to surpass T2w-MRI in the detection of recurrent disease.

To successfully develop focal salvage strategies for recurrent PCa, an accurate detection and localisation of the tumour as well as distinction from radiation affected benign tissue is necessary.

The objectives of this study were to: 1) investigate RT-induced tissue changes and how these impacted the distinction of recurrent tumour from surrounding benign tissue; and, 2) use quantitative sequences to characterise both benign tissue and recurrent PCa after RT, and investigate which sequences resulted in optimal tumour localisation.

4.2 MATERIALS AND METHODS

4.2.1 Patient Recruitment and Matching

This prospective single–institution study was approved by the Institutional Re–view Board and took place between December 2015 and July 2018. All patients signed informed consent prior to participation in the study. An overview of the study design can be seen in **Figure 4.1**.
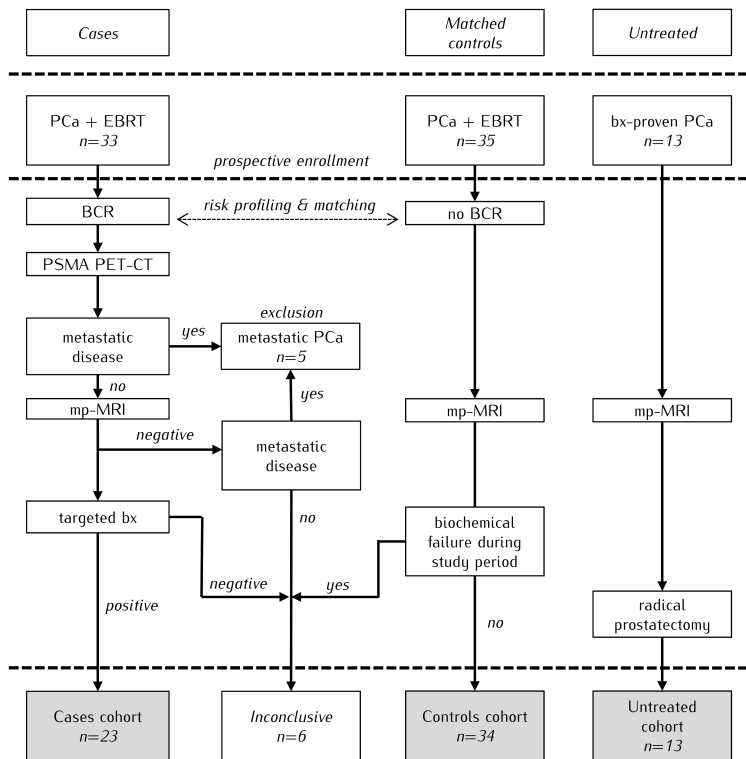
Figure 4.1: Study design with an overview of the three analysed cohorts. BCR, biochemical recurrence; bx, biopsy; EBRT, external-beam radiation therapy

Cases (patients with recurrent PCa)

Patients with a biochemical recurrence according to the Phoenix definition [65], were enrolled in the study. Patients could only be included more than 24 months after completion of EBRT and if they qualified for salvage treatment. A gallium-68 prostate-specific membrane antigen positron emission tomography (^{68}Ga-PSMA-PET) scan was acquired to exclude metastatic disease. Exclusion criteria were hormonal therapy in the past year, the use of anticoagulants that could not be stopped temporarily to acquire biopsies, contra-indications for an MRI exam and other treatments for cancer in the pelvis. Patients received a mp-MRI. When a tumour suspected region was identified, an MR-fused ultrasound-guided biopsy was performed targeting this region. If no tumour suspected region could be identified, either only prostate-specific antigen (PSA) follow-up would be continued or a standard systematic biopsy could be performed. This decision was made by the treating physician. Patients with positive imaging and biopsy findings for locally recurrent PCa constituted the cohort of case patients.

An inconclusive diagnosis was given to patients for whom a local or metastatic recurrence could not be detected on MRI, or the biopsies were negative or both. These patients were analysed further but separately from the cohort of cases.

Controls (patients without recurrent PCa)

Matched controls (patients without evidence of recurrent disease) were recruited and received a mp-MRI scan. The matching criteria were: time since primary RT (years), use of hormonal therapy and the risk group of the primary tumour. Risk stratification was based on the definition proposed by the European Association for Medical Oncology (ESMO) in 2010 [119], incorporating changes suggested in the review by Rodrigues *et al.* [120] on the importance of the amount of high-grade cancer, differentiating between Gleason 3+4 and 4+3. Risk stratification was defined as: low-risk - T1-T2a, Gleason $\leqslant$ 6 and PSA $\leqslant$ 10 ng/ml; intermediate-risk – T2b-T2c, Gleason = 7 (3+4) and PSA $\leqslant$ 20 ng/ml, not otherwise low-or high-risk; high-risk - T3-T4 or Gleason $\geqslant$ 7 (4+3) or PSA >20 ng/ml. The exclusion criteria were identical to those applied for the cases.

If a patient developed a biochemical recurrence during the study period, he was moved to the inconclusive cohort.

Untreated (patients at primary diagnosis)

A previously reported cohort of 13 primary PCa patients [121, 122], scanned prior to treatment with a mp–MRI protocol, was used as reference. As part of the study, these patients underwent two mp–MRI scanning sessions. Following the second MRI examination, the patients were treated with a radical prostatectomy. This cohort is referred to as the untreated cohort.

4.2.2 MRI Protocol

All patients were scanned in a 3T Achieva dStream (A) or Ingenia (B) scanner (Philips Healthcare, Best, The Netherlands). Twenty patients were scanned in system A with a 6–channel cardiac coil and 48 were scanned in system B with a 16–channel anterior and 12–channel posterior coil. With the exception of 4 patients (3 scanned in system A), all were scanned with the use of an endorectal coil.

The mp–MRI protocol consisted of an axial, sagittal and coronal T2w turbo spin echo; a 3D gradient echo T1–weighted (T1w); a balanced steady–state free precession (bSSFP); an axial multi–echo spin echo k–t–T_2 sequence [121], with twelve echoes acquired at a spacing of 16ms, starting at 32ms; a transversal diffusion weighted sequence (DWI) and a dynamic contrast–enhanced sequence (DCE). DWI was acquired using a single–shot spin–echo echo–planar imaging sequence with diffusion encoding b–values ranging from 0 to 800 sec/mm^2. DCE was acquired with a 3D T1w spoiled gradient echo sequence at a temporal resolution of 2.6 seconds over 5 minutes, before, during and after intravenous administration of 15 ml of Dotarem (0.5 mM Dotarem, Guerbet, Roissy CDG, France). The contrast agent was administered using a power injector (MedRad, Warrendale, PA, USA), followed by a 30 ml saline flush at a flow rate of 3 ml/sec. Further sequence specific details can be found in **Table S4.1** (Supplementary Materials).

Apparent diffusion coefficient (ADC) maps were derived from the DWI sequence using $b = 200$ and 800 sec/mm^2. The standard Tofts model [123] was used to calculate the pharmacokinetic maps K^{trans} and k_{ep}. This was done using a T_1 map generated based on the variable flip angle method [124], using flip angle = 3 °, 6 °, 10 °, 20 °, and 30 °, to convert signal intensity into concentration, and an arterial input function (AIF) with parameters derived from an in-house study population. T_2 maps were created by converting the signal to the logarithmic scale and performing a weighted linear fit.

All sequence-derived functional maps were generated using MATLAB R 2017b (Mathworks, Natick, MA, USA).

Visual inspection was used to assess possible displacements between the functional sequences (and respective quantitative maps) and the T2w-MRI scans. Rigid registration based on mutual information was used whenever necessary to correct for these displacements. All images were resampled to the T2w grid.
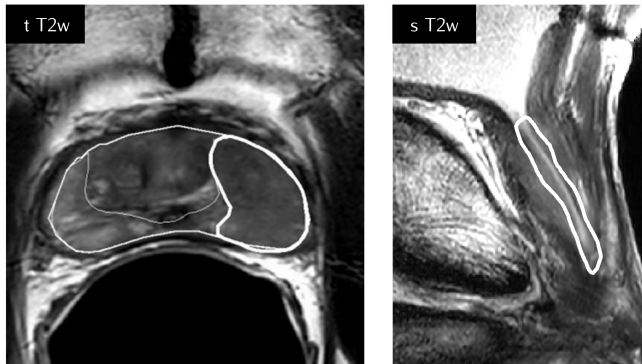

Figure 4.2: Illustration of the delineated ROIs. In the left image the eroded prostate contour, the peripheral zone, and the tumour can be seen delineated on the transversal T2w image. On the right, the peri-urethral contour is presented overlaid on the sagittal T2w scan.

4.2.3 Region of Interest (ROI) segmentation

The prostate, the peripheral zone (PZ), the central gland (CG) and the region surrounding the urethra – peri-urethral tissue (PU) – were delineated. The PU region was delineated using both the sagittal and transversal T2w images. The tumour suspected regions were delineated by a radiologist (14 years of experience) based on the MRI, PET and biopsy report information. As the Prostate Imaging Reporting and Data System 2 (PI-RADS v2) [42] is not applicable to recurrent prostate cancer, tumour was defined as a region with low signal-intensity (SI) on T2w-MRI, high SI in the b=800 DWI scan, low SI on the ADC map, and increased enhancement in the K^{trans} and k_{ep} maps. For the untreated cohort tumour delineations were originally performed on the histopathology and propagated to imaging. **Figure** 4.2 illustrates the ROIs as delineated for a case patient.

The bSSFP sequence was used to identify and exclude from further analysis the implanted fiducial markers. Prostate delineations were eroded in all directions by 1mm to ensure that only prostate tissue was analysed.

Region of interest (ROI) analysis was performed using Python 3 (Python Software Foundation, Delaware, United States).

4.2.4 Statistics

A t-test for continuous variables (PSA) and a chi-square test for categorical variables (Gleason and TNM stage) were used to compare the clinical characteristics of the cohorts.

Normality was checked using the Shapiro Wilk test. In a case of non-normality a non-parametric Friedman's ANOVA for dependent groups was used to compare the different regions within the groups (untreated, cases and controls). If significant, the differences were further evaluated using a post-hoc Wilcoxon signed-rank test. To compare the same region between groups, a Mann-Whitney test was used. To correct for multiple testing, a Bonferroni correction was applied to the significance level of $\alpha = 0.05$.

Univariate and multivariate generalised linear mixed–effect modelling (GLMM) was applied to assess the predictive value of imaging on the voxel–wise likelihood of tumour. Only case patients were used in this analysis. Voxels were grouped into benign (resulting from a combination of unaffected PZ and CG) and tumour (based on the radiologist delineations). To obtain the likelihood of tumour on a voxel level, fixed and random effects were included. The quantitative imaging maps and voxel anatomical location (PZ or CG) were accounted as predictive variables and therefore included as fixed effects. Random effects accounted for spatial clustering by incorporating voxel location within the prostate (the relative distance in x, y and z from the prostate centre of mass) and patient identifiers. When the association between model parameters and tumour probability was non–linear, the parameters were grouped in quartiles and regression coefficients were estimated for each group considering the first quartile as reference. The model fit was assessed using the Bayesian Information Criterion (BIC) (a decrease of 10 points reflects an improved fit) and by evaluating the residual random error. Statistics were performed with the Statistical Package for Social Sciences, version 22.0 (SPSS, Chicago, IL, USA). Analysis was performed in R [125] using the lme4 package [126].

4.3 RESULTS

4.3.1 Patient Characteristics

In total, 33 case patients and 35 controls were prospectively included in the study. Adjuvant hormonal therapy was given for a maximum period of 3 years to 82% of the cases and to 94% of the controls upon the treatment of primary PCa. However, none of the patients received hormonal therapy within 1 year prior to the MRI exam.

Cases (patients with recurrent PCa)

Ten of the 33 included patients had either regional metastases without evidence of intraprostatic recurrence (n=5) or an inconclusive diagnosis (n=5). Twenty-three patients remained that fitted all the inclusion criteria for cases. For 3 of the 23 case patients, the first biopsy was negative and a repeated navigated biopsy confirmed the MRI suspected tumour location.

In 2 out of 23 patients the k–t–T_2 sequence was not acquired and for another the ADC map was not used due to poor image quality.

For the 23 cases a total of 27 suspected tumour foci were delineated, with an average tumour volume of 1.37 cm^3. From these, 4 were located in CG. The median time to recurrence for the 23 cases was 7 years since primary EBRT treatment.

Controls (patients without recurrent PCa)

One patient was initially recruited as a control but had a biochemical failure during the study period. This patient was moved to the inconclusive cohort. The remaining 34 matched controls (patients without evidence of locally recurrent PCa) had a median time of 6 years since the EBRT treatment.

Untreated (patients at primary diagnosis)

The 13 untreated patients had a median time of 20 (range, 5–65) days between the MRI and prostatectomy. None of these patients received hormonal therapy before imaging. For one patient, the small dimensions of the histopathological tumour resulted in a sub–voxel tumour ROI in MRI. For this patient only benign tissue was analysed.

Table 4.1 describes the patient characteristics for cases, controls and untreated patients. For the untreated patients, the characteristics reported in the table are based on the biopsy report and clinical TNM stage.

The clinical characteristics of the cohorts were compared. TNM stage was grouped in two (T1+T2 and T3+T4) and the Gleason score in three groups (Gleason $\leqslant$ 6, 7, $\geqslant$8). Cases and controls had comparable clinical characteristics (PSA: p=0.789; TNM stage: p=0.393; Gleason score: p=0.271). Both case and control patients had significantly higher-risk primary PCa when compared with the untreated patients (PSA: p=0.008 and p=0.003; TNM stage: p=0.004 and p<0.001; Gleason score: p=0.03 and p=0.004 for cases and controls, respectively).

Figure 4.3 illustrates the values of T_2, ADC, K^{trans} and k_{ep} for untreated, controls, and case patients. Median imaging values for the 3 cohorts are presented in **Table** 4.2.

Table 4.1: Patient characteristics. Recurrent tumours were not assigned a Gleason score as radiation induced atypia can be a confounder for pathological interpretation.
In six case patients TNM stage of recurrent tumour was not reported
† *For one case patient only the Anderson score (=2) was available*
‡ *In one case and one control the PSA of the primary tumour could not be retrieved*

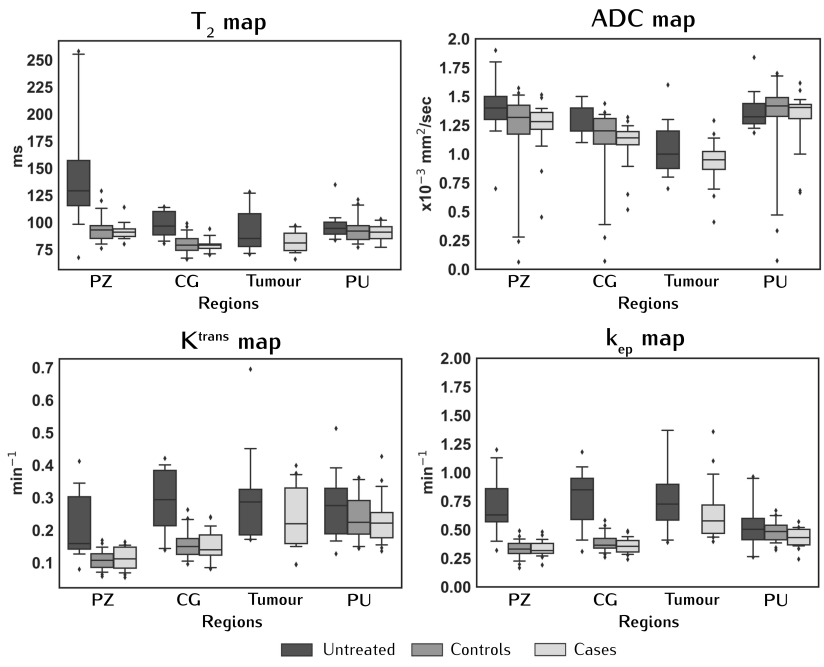|	Cases		Controls	Untreated
	Primary tumour	Recurrence	Primary tumour	Primary tumour
TNM stage *				
T1	-	-	5	5
T2	11	13	6	7
T3	11	4	23	1
T4	1	-	-	-
Gleason score †				
$\leqslant$ 6	4	-	6	7
7	12	-	12	6
$\geqslant$ 8	6	-	16	-
PSA (ng/ml) ‡				
$\leqslant$ 10	10	22	11	12
10 <PSA $\leqslant$ 20	6	1	14	1
$\geqslant$ 20	6	-	8	-

Figure 4.3: Boxplots with median values for all regions, imaging modalities, and the three cohorts of patients: untreated, controls (non-recurrent), and cases (recurrent). Edges of the boxes are the first (25th) and third (75th) quartiles, and whiskers represent the 5th and 95th percentile. PZ, peripheral zone; CG, central gland; PU, periurethral tissue.

Table 4.2: Quantitative imaging values for the three cohorts in the different prostatic regions. Median of all individual patients' median values, with the minimum and maximum presented between brackets.

		PZ	CG	Tumour	PU
T_2 (ms)	Untreated	129 (67-258)	97 (81-114)	85 (70-128)	94 (84 - 135)
	Controls	93 (76-129)	79 (66-99)	-	92 (77-121)
	Cases	91 (80-114)	79 (70-94)	81 (66-97)	91 (77-103)
ADC ($\times 10^{-3}$ mm^2/s)	Untreated	1.40 (0.70-1.90)	1.20 (1.10-1.50)	1.00 (0.70-1.60)	1.32 (1.20 - 1.80)
	Controls	1.32 (0.06-1.57)	1.20 (0.07-1.44)	-	1.41 (0.07-1.70)
	Cases	1.28 (0.45-1.51)	1.14 (0.52-1.32)	0.95 (0.41-1.29)	1.40 (0.67 - 1.62)
K^{trans} (min^{-1})	Untreated	0.16 (0.08-0.41)	0.29 (0.14-0.42)	0.29 (0.17-0.70)	0.28 (0.13-0.51)
	Controls	0.11 (0.06-0.17)	0.15 (0.10-0.26)	-	0.22 (0.14-0.36)
	Cases	0.11 (0.05-0.16)	0.14 (0.08-0.24)	0.22 (0.09-0.40)	0.22 (0.14-0.43)
k_{ep} (min^{-1})	Untreated	0.63 (0.32-1.20)	0.85 (0.31-1.18)	0.73 (0.39-3.89)	0.50 (0.26-0.96)
	Controls	0.33 (0.17-0.49)	0.37 (0.26-0.58)	-	0.48 (0.32-0.67)
	Cases	0.32 (0.19-0.48)	0.36 (0.24-0.49)	0.58 (0.40-1.36)	0.43 (0.24-0.57)

4.3.2 Characteristics of irradiated benign tissue

Figure 4.4 illustrates the quantitative maps and suspected tumour regions for a representative case (**Figure 4.4**A) and control (**Figure 4.4**B) patients.

The values for benign PZ and CG were comparable between cases and controls (P = 0.15 for ADC in the CG up to 0.91 for the k_{ep} in the PZ). Values in the PU were also similar between the groups (with the lowest P = 0.05 for k_{ep} > 0.05/3). Both cases and controls presented with PU enhancement.

For controls, significant differences were found between PZ and CG and between CG and PU (P < 0.001 for all comparisons between imaging values and regions).

The values obtained for the PZ, CG and PU in the inconclusive cohort were not significantly different from those of the cases (with the lowest P = 0.03 for T_2 in the PZ > 0.05/3) or controls (with the lowest P = 0.04 for T_2 in the CG

$> 0.05/3$). The quantitative imaging values for this specific cohort are present in the **Table S4.2** (Supplementary Materials).
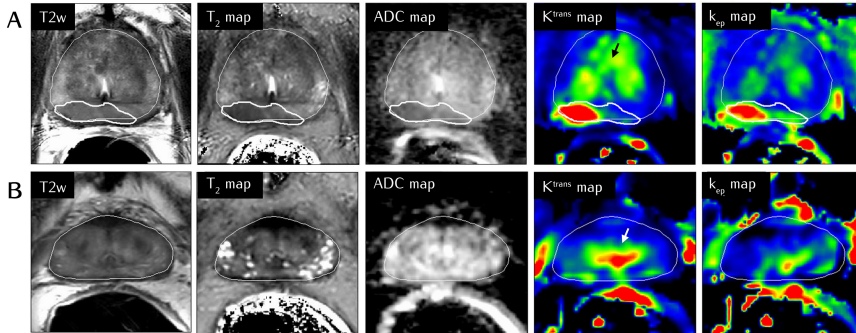

Figure 4.4: Representative example of a case (A) patient with recurrence and a control (B) without recurrent disease, with all anatomical and functional maps. Thin and thick white lines represent prostate and tumour delineations, respectively. Black and white arrows in the K^{trans} maps point to the increased enhancement in the peri-urethral tissue, present in both cases and controls.

4.3.3 Radiation-induced changes

To investigate radiation-induced tissue changes, the values from the untreated patients were used as a population reference against which the values of the cases were compared.

The different prostate regions were more homogeneous after RT and the range of values was in general smaller than before treatment. With the exception of ADC (for which $P = 0.03 > 0.05/4$), T_2, K^{trans} and k_{ep} values in the PZ were significantly lower (T_2, k_{ep} $P < 0.001$ and K^{trans} $P = 0.002$) after RT. The CG imaging values were for all maps significantly lower after RT (all with $P \leqslant 0.001$). In the PU, despite the higher K^{trans} values seen before treatment, the imaging values for all maps remained comparable before and after treatment ($P = 0.19$ for T_2 up to $P = 0.56$ for ADC).

Similar characteristics were seen for all maps for recurrent and primary tumours ($P = 0.17$ for k_{ep} up to $P = 0.22$ for ADC).

4.3.4   Tumour localisation

To compare recurrent tumour with the remaining irradiated benign gland, the cohort of case patients was assessed. With all imaging maps, median tumour values were significantly different from benign tissue within the PZ (P < 0.001 for all imaging modalities). No differences were seen between the T_2 values of suspected tumour and benign CG tissue (P = 0.08). However, values of ADC, K^{trans} and k_{ep} from suspected tumour regions were significantly different (all with P < 0.001) from those of the CG. When compared with the surrounding benign tissue, heightened K^{trans} and k_{ep} values were seen in the PU. The PU K^{trans} values were comparable with those of suspected tumour (P = 0.81), but with k_{ep} a significant distinction (P < 0.001) could be made between the two regions. The PZ and CG ROIs were significantly different for all maps except k_{ep} (P = 0.05 > 0.05/6).

Table 4.3: Model parameters obtained when combining T_2 map, ADC, K^{trans} and k_{ep} imaging values to predict tumour at the voxel-wise level. Imaging values and location are included as fixed effects; patient and spatial coordinates as random effects.

Fixed effects (MRI)	Regression coefficients (β)	Std. Error	P
T_2 map reference group (24 – 73)	0	-	-
T_2 map 2nd quartile (74 – 83)	0.08	0.01	<0.001
T_2 map 3rd quartile (84 – 97)	-0.40	0.01	<0.001
T_2 map 4th quartile (98 – 1188)	-1.50	0.02	<0.001
ADC	-2.86	0.02	<0.001
K^{trans}	6.52	0.09	<0.001
k_{ep}	4.85	0.04	<0.001
Location	-0.98	0.01	<0.001
Intercept (β_0)	-5.55	0.46	<0.001

Random effects	Variance (σ^2)		
Patients	1.41		
Distance CM_x	0.67		
Distance CM_y	8.50		
Distance CM_z	13.30		

Residuals (ϵ_0)	Median	First quartile	Third quartile
	-0.07	-0.13	-0.03
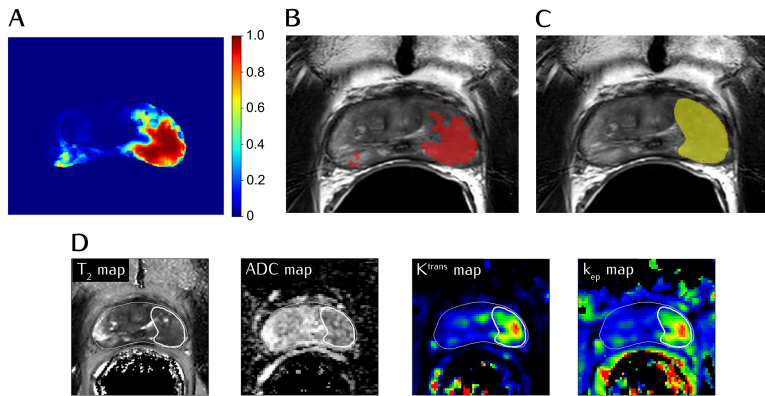
Figure 4.5: A reconstructed probability map based on the generalised linear mixed model (A). In red, overlaid on the T2w scan (B), is the same probability map thresholded at 0.5 and in (C), in yellow, the original tumour delineation. The anatomical and functional maps are presented in (D), together with the prostate and tumour delineations in white.

Using the GLMM, we observed that univariately all MRI parameters were significantly associated with tumour likelihood ($P < 0.001$). Location within the gland was also significantly associated with tumour likelihood. The association between T_2 and tumour probability was non-linear, and therefore this parameter was grouped in quartiles with univariate regression coefficients $\beta = 0$ (reference group), 0.19, -0.59 and -1.83. The regression coefficients were for ADC: $\beta = -5.06$, K^{trans}: $\beta = 17.27$, k_{ep}: $\beta = 8.42$ and location: $\beta = -0.64$. The multivariate model combining all mp-MRI parameters and location obtained the best fit and was the most predictive for tumour likelihood (BIC of 392212, $P < 0.001$). The values for the regression coefficients and standard errors are presented in **Table 4.3**. A reconstructed probability map for a case patient is presented in **Figure 4.5**.

4.4   DISCUSSION

In this study mp-MRI was used to quantitatively describe and distinguish benign prostate tissue from recurrent PCa after RT. The use of two patient cohorts,

with and without recurrent PCa, allowed us to show that tumour unaffected areas were similar in both groups. Compared with the pre-treatment setting, and with exception of ADC in the PZ, all other imaging values (T_2, K^{trans} and k_{ep}) were lower, but also more homogeneous between the PZ and CG. This is in agreement with literature describing the loss of zonal distinction in the post-RT setting [37]. Still, significant differences between the imaging values of PZ and CG were seen in both recurrent and non-recurrent patients. As in primary disease, recurrent tumour occurred predominantly in the PZ. This is not surprising as recurrence usually happens at the site of primary PCa [55]. For all maps, values of recurrent tumour were not significantly different from those of primary PCa.

With all imaging maps, we found that the PZ was significantly different from recurrent tumour, illustrating that all quantitative maps seem to have potential to distinguish tumour in this region. However, tumour detection in the CG is challenging using solely the T_2 map, as the values for benign CG and tumour are not significantly different. This distinction is possible when evaluating ADC, K^{trans} and k_{ep}. The PI-RADS v2 [42] is the standard radiological guideline for the diagnose of primary PCa. These guidelines do not apply to the detection of suspected recurrent PCa following treatment. Yet, in the absence of further guidance, PI-RADS v2 is often used as a starting point for image assessment. The guideline describes T2w as the dominant mp-MRI sequence for the diagnosis of primary PCa in the transition-zone. Our results suggest this sequence is of less relevance compared to the other mp-MRI sequences when diagnosing recurrent PCa in this region. The results also suggest that DCE-MRI has an important role in the diagnosis of recurrent disease. In non-irradiated prostate tissue, the presence of benign prostatic hyperplasia (BPH) in the central gland is an important imaging confounder for the use of DCE-MRI in this region. In a previous study, pathology slides from salvage prostatectomy specimens of recurrent PCa patients after radiotherapy were registered to mp-MRI acquired prior to the surgery. In the analysed pathology, no BPH could be found [127]. This suggests that BPH vanishes after radiotherapy. The enhancement in the peri-urethral area remains and needs to be considered. It has been hypothesised that the fibrotic changes observed in irradiated prostates [128] and the decreased microvasculature associated with atrophic tissue, enhance the neovascularity of recurrent tumour relative to the remainder benign atrophic tissue [43].

With overall median values below 100ms, T_2 is decreased for the prostate as a whole after RT. Measured T_2 values (ms) were in agreement with a previous study observing the effects of RT in prostate tissue [129] (at week 8 of the RT treatment, mean $\pm$ SD: PZ = 89 $\pm$ 13, CG = 76 $\pm$ 5, Tumour = 75 $\pm$ 9) and they provide evidence that the PZ and CG values do not increase after these 8 weeks.

The ADC values (in x 10^{-3} mm^2/sec) obtained for recurrent tumour were similar to those reported in other studies (mean $\pm$ SD: 1.0 $\pm$ 0.1 and 0.98 $\pm$ 0.23) [130, 131]. Tumour values in the untreated cohort were also comparable to those previously described (tumour PZ, mean $\pm$ SD: 1.08 $\pm$ 0.39) [132]. Values for benign prostate tissue in our case and control cohorts were slightly lower than those reported by others (mean $\pm$ SD: 1.6 $\pm$ 0.2 and 1.60 $\pm$ 0.21; x10^{-3} mm^2/sec) [130, 131]. We note that these studies did not distinguish PZ from CG and reported values for a composite of both regions. In our untreated cohort, benign prostate tissue showed slightly lower values than those seen by Sato *et al.* (mean $\pm$ SD: 1.80 $\pm$ 0.41 for PZ and 1.58 $\pm$ 0.37 for the transition–zone) [132].

In controls the PU region exhibited high K^{trans} and k_{ep} values without signs of malignancy. Similar high values were found in cases and this enhancement strongly overlapped with tumour values, which might represent a confounder for tumour detection in the CG. Yet, with k_{ep} significant differences were seen between tumour and PU, suggesting this could be a relevant parameter when assessing the CG. This effect has been previously described in the recurrent setting [38, 44], potentially as a result of remaining BPH or peri–urethral vasculature. Donati *et al.* [46] found no additional benefit of DCE when complementing T2w and DWI, which could have been the result of benign CG enhancement.

The GLMM analysis revealed tumour distinction was optimised with the use of mp–MRI, highlighting the importance of using a combination of anatomical and functional sequences when identifying and localizing tumour for salvage treatment strategies. Our study did not include spectroscopic data. Nonetheless, spectroscopic data has been suggested as a valuable tool for recurrent tumour distinction [130].

Quantitative tissue characterization enables a more straightforward comparison between subjects, studies and centres. It also conveys important information to adapt the scanning protocols to better image this study population. As an example, for patients with suspected recurrence, the sampling echo times for T_2 mapping should be shortened as T_2 decay is expected to be shorter compared to untreated patients.

We aimed to circumvent the limitations of a 2D standard transrectal ultrasound (TRUS)-guided systematic biopsy by using a 3D MRI-TRUS fusion approach to target the tumour suspected region. With this technique's improved spatial information, it has been described that fewer cores were necessary to detect more clinically significant cancer [133], often leading to reclassification of primary tumours in higher risk categories [134]. Nonetheless, for a subset of our patients, cancer was only confirmed with repeated biopsy. Even when navigated, the biopsy procedure is limited by possible co-registration errors and in delivering the biopsy needle to the intended point [135]. Tumour delineations performed using 1.5T T2w, were shown to underestimate the true tumour volume when compared with prostatectomy samples [55]. As a result, the detection rates of MRI-TRUS fusion biopsies might also be affected by errors in defining the lesion to target.

Our study has several limitations. Firstly, it was a single hospital study with a limited number of patients. The controls were recruited to match the characteristics of cases as best as possible, and no significant differences were seen between their clinical parameters. However, our cohort of cases and controls had significantly higher-risk primary PCa when compared with the untreated patients. Thus, the reported imaging differences for benign tissue could theoretically arise from baseline imaging dissimilarities. No significant imaging differences were seen between the tumours in the untreated and recurrent cohorts.

Ideally, using salvage prostatectomy specimens as the standard of reference would be preferred to accurately identify cancer location, but this procedure is only sporadically performed. Thus, patients with an inconclusive diagnosis were analysed separately to avoid a potential bias. The diagnosis of recurrent disease is in practice made with a combination of mp-MRI and PSMA-PET findings. In this study we opted to individually investigate the properties of

MRI which, due to its higher spatial resolution, is better suited for the purpose of tumour localisation. A combination of both modalities can certainly help better select patients suitable for salvage treatment. Lastly, our GLMM was not tested in an independent cohort. Thus further validation is required to establish applicability to other populations. The model is also potentially reflecting delineation practices.

In conclusion, tumour unaffected areas were similar between recurrent and non-recurrent patients, and generally with lower and more homogeneous values than before RT. The PU region presents with increased enhancement in the pharmacokinetic maps for both cases and controls. Analysis of mp-MRI, with the quantitative maps T_2, ADC, K^{trans} and k_{ep} together with location information resulted in optimal distinction between tumour and benign voxels. The ability to accurately localise tumour and distinguish it from benign tissue with the use of mp-MRI will help in the design of focal salvage treatment strategies for locally recurrent PCa.

SUPPLEMENTARY MATERIALS

Table S4.1: Sequence specific parameters.

Two case patients were scanned using a different protocol. T2w had a TR (ms) = 3952 and 3969 and TE (ms)= 120ms, with a reconstructed voxel size of 0.4 × 0.4 × 3 mm³. T1w had TR (ms) = 3.61 and 3.67 and TE (ms) = 1.80 and 1.85, and a reconstructed voxel size (mm) of 0.85 and 0.84 with a 2mm slice thickness. The DWI sequence had a TR (ms)= 5355 and 4931 and a TE (ms) = 61.8 and 54.0, with a reconstructed voxel size of 1.06 × 1.06 × 3 mm³. For these patients a balanced TFE and k-t-T2 sequences were not acquired. The DCE sequence was the same as described in the table above.

	Imaging plane	Scan mode	Field of view (mm)	Matrix size	Slice thickness (mm)	Reconstructed voxel size (mm)	TR/TE (ms)	Echo train length	Flip angle (degrees)	Acceleration factor	Receiver bandwidth (Hz/voxel)	Phase encoding direction	Acquisition time	Number of signal averages
T1 THRIVE	Axial	3D	280 × 448	448 × 378	2.0	0.88	3.7 / 1.86	88	10	halfscan = 0.6 & SENSE factor 1	720	RL	2min 42sec	3
T2 TSE	Axial	2D	140 × 140	304 × 242	3.0	0.27	3143 / 120	26	90	N/A	236	RL	3min 2sec	1
k-t-T_2	Axial	2D	170 × 170	212 × 212	3.0	0.39	2469 / 32; ΔTE = 16	12	90	SENSE factor 2	169	RL	5min 6sec	1
DWI	Axial	2D	160 × 180	144 × 144	2.7	1.03	3131 / 55	49	90	SENSE factor 2	17.2	RL	2min 23sec	1, 4, 8 for b=0, 200, 800
DCE	Axial	3D	260 × 260	144 × 144	6.0	1.16	4.0 / 1.9	1	20	SENSE factor 4	2117	RL	4min 56sec	1
bTFE	Axial	3D	250 × 250	252 × 234	2.0	0.49	3.70 / 1.85	36	30	N/A	1240	RL	2min 23sec	1

Table S4.2: Median of all patient's median values for each region and imaging sequence for the inconclusive cohort. Minimum and maximum values are presented between brackets.

	Inconclusive		
	PZ	**CG**	**PU**
T_2 ms	84 (76 - 100)	70 (62 - 82)	83 (76 - 111)
ADC $\times 10^{-3}\ mm^2/s$	1.31 (1.20 - 1.48)	1.13 (1.03 - 1.36)	1.39 (1.16 - 1.68)
K^{trans} min^{-1}	0.09 (0.04 - 0.12)	0.14 (0.08 - 0.24)	0.19 (0.12 - 0.25)
k_{ep} min^{-1}	0.29 (0.12 - 0.33)	0.33 (0.21 - 0.40)	0.43 (0.28 - 0.50)